(article starts on next page)

METHODS ARTICLE

Linking cell design and production energy demand to estimate environmental impacts of NMC lithium-ion batteries

Mudit Chordia[1] | Evelina Wikner[2] | Anders Nordelöf[1,3] | Ketan Vaidya[4] |
Rickard Arvidsson[1]

[1]Division of Environmental Systems Analysis, Chalmers University of Technology, Gothenburg, Sweden

[2]Division of Electric Power Engineering, Chalmers University of Technology, Gothenburg, Sweden

[3]The Swedish National Road and Transport Research Institute, Gothenburg, Sweden

[4]Northvolt AB, Stockholm, Sweden

Correspondence
Mudit Chordia, Division of Environmental Systems Analysis, Chalmers University of Technology, Gothenburg, Sweden.
Email:mudit@chalmers.se

Editor Managing Review: Lynette Cheah

Abstract

Life cycle assessment of several common lithium-ion battery (LIB) cell designs is hindered by lack of cell-specific large-scale production data. This issue is further exacerbated by the fact that automotive manufacturers deploy diverse LIB cell types optimized to meet specific application demands through variations in chemistry, internal design, and format, posing significant challenges in assessing the environmental impacts of different cell types. To address this, this study proposes a parameterization methodology that links cell design parameters, such as electrode and casing area, and cell energy with production processes to investigate the influence of cell type on climate and resources impacts. The parameterization methodology is applied across 14 cell types employing graphite and nickel manganese cobalt oxide electrodes, varying in format, internal design, and nickel content. Results reveal substantial variability in energy demand during production when reported per cell, ranging from 1 to 30 kWh/cell for electricity and 2 to 50 MJ/cell for cooling. When reported per kWh_{cell} the variation is smaller, 61–63 kWh/kWh_{cell} for electricity and 107 MJ/kWh_{cell} for cooling. Impacts of power-optimized cells are higher than energy-optimized cells due to larger negative electrodes of the former. Cylindrical cells have lower impacts than prismatic cells owing to their superior volumetric efficiency. Higher volumetric efficiency of single- over four-jelly rolls in prismatic cells also yielded lower impacts. Thus, pointing to the importance of internal cell design when assessing environmental impacts. Finally, higher-nickel-content chemistries exhibit reduced climate and resource impacts due to a decreased reliance on cobalt which has higher impact during extraction and production.

KEYWORDS
climate change impacts, life cycle assessment, lithium-ion batteries, parameterization, resource use impacts, scaling

1 | INTRODUCTION

Battery electric vehicles (BEVs) are promoted as an alternative to fossil fuel-based internal combustion engine vehicles. Lithium-ion batteries (LIBs) are currently the most common choice of energy storage technology for electric vehicle application (IEA, 2024) because they offer high energy density, high voltage, low self-discharge rate, long cycle life, and high charging and discharging rate capability (Ding et al., 2019). Life cycle assessment (LCA) studies have pointed to the production of LIBs as energy intensive and having high environmental impacts in the life cycle of the BEVs (Bouter & Guichet, 2022). However, improvements in production technology, large-scale production, coupling battery production to low-carbon intensive energy sources, and increasing share of recycled content for several key battery materials have reduced the environmental impacts from LIB production, in turn lowering the overall impacts of the BEV life cycle (Chordia et al., 2021; Sankar et al., 2023).

In the current LIB technology, there are several cell chemistries (electrode active materials and electrolytes) and formats (geometry) being implemented (Perner & Vetter, 2015). Commonly used cell formats are cylindrical, prismatic, and pouch (Birke & Demolli, 2018). Within each cell format, multiple cell configurations can be designed by optimizing the dimensions of the active parts of the cell, cell chemistry, and internal design. As such, there are many cell types that are possible for implementation in BEV applications (Chabot et al., 2013; Shin & Lee, 2024). While the most common negative active material (NAM) is graphite, there is a larger variation in the positive active material (PAM) (Mekonnen et al., 2016). Some examples of PAMs used in LIBs are lithium nickel manganese cobalt oxide (NMC), lithium nickel cobalt aluminum oxide (NCA), lithium cobalt oxide (LCO), and lithium iron phosphate (LFP). Within the NMC cell chemistry, there are several variants with varying shares of nickel, manganese, and cobalt. Some common variants are NMC111, NMC532, NMC622, and NMC811 (Noh et al., 2013). Increasing the nickel content and thereby lowering the manganese and cobalt share improves the energy density and power capability and lowers the cost of the LIB cells (Manthiram, 2017).

LCA is a commonly applied methodology to assess the environmental impacts of LIB production and for identifying the environmental hotspots in the supply chain (Chordia, Wickerts et al., 2022; Istrate et al., 2024; Kallitsis et al., 2024). LCA studies require inventory data that specifies material, energy, wastes, and emissions from the production processes. However, as primary inventory data representing different cell types is difficult to acquire, LCA studies adapt unit process datasets from existing studies for their own inventory modeling. While this is a common practice to manage data gaps in LCA studies, it impedes in developing a nuanced understanding of how cell type affects environmental impacts. This is particularly relevant when trying to understand the links between cell design parameters and energy demand. For instance, in their reviews, Kallitsis et al. (2024) report energy demand in the range of 40–80 kWh/kWh cell storage capacity (hereafter referred as kWh/kWh$_{cell}$), while Bouter and Guichet (2022) report 10–70 kWh/cell across various LCA studies on LIB production. The reviews cover LCA studies assessing different cell types, but exactly how the cell type influences energy demand in cell production is not clear. Further, LCA studies also need to consider future changes in cell production, such as technological advancements in manufacturing and the implementation of new cell types. Addressing this gap is crucial for guiding the development of LIBs and other emerging battery technologies toward reduced environmental impacts.

Several recent studies have contributed to understanding differences in energy demand in cell production. For example, Jinasena et al. (2021) use physics-based equations to calculate energy demand for cell assembly, production processes, and factory utilities, representing a 2 GWh/year facility producing NMC333 prismatic cells. They calculate a total energy demand of 47 kWh/kWh$_{cell}$ reported as electricity, although they state the heating and cooling are included in this demand. They further calculate the energy demand for producing other NMC cells and report a range of approximately 35–55 kWh/kWh$_{cell}$. However, the authors do not specify the share and source of heat and cooling. Degen and Schütte (2022) utilize machine power ratings obtained from equipment manufacturers to estimate factory throughput based on the machine with the lowest reported production capacity, assuming it serves as the limiting factor in production processes. They estimate an electricity demand of 20 kWh/kWh$_{cell}$ and a heat demand of 75 MJ/kWh$_{cell}$ (from natural gas) for producing a 21700 NMC622 cell in a 7 GWh/year facility. In a follow-up study, Degen et al. (2023) report the energy demand in production for a range of NMC cells of approximately 9–15 kWh/kWh$_{cell}$ electricity and 35–60 MJ/kWh$_{cell}$ heat. Knehr et al. (2024) used the recently updated BatPaC model (v5.1) and regression analysis to link energy demand in cell production with cell design parameters, by determining the linearity of the production scaled relative to the power rating of the processing equipment. They report an electricity demand of around 35 kWh/kWh$_{cell}$ and 25 MJ/kWh$_{cell}$ of heat from natural gas, for production facility sizes of 5–50 GWh/year producing NMC83 pouch cells. The scaling relationships in Knehr et al. (2024) are derived based on regressions for pouch cells only, and do not capture physical relationships between different cell types and energy use. The range in their energy demand values for the reference cell correspond to effects due to economies of scale. Furthermore, LCA studies such as Jinasena et al. (2021), Degen and Schütte (2022), and Knehr et al. (2024) represent what can be called a bottom-up approach to inventory modeling. Such modeling approaches generally utilize process-specific data which likely implies higher precision in modeling energy demand. In a more recent work, Clos, Ventura Silva et al. (2025) propose a scalable energy model incorporating over 20 cell and process parameters derived from an automated pilot line and employ a bottom-up approach to modeling energy demand and a top-down approach to material demand. In further development of the scalable energy model, Clos, Baars et al. (2025) present an automated LCA and cost modeling platform using the CellEst tool (Greenwood et al., 2021). They report results by chemistry only and not cell type. Baars et al. (2023) on the other hand model energy demand indirectly, scaling it with battery mass and energy density using fixed Wh/kg factors provided in Degen and Schütte (2022). However, the risk in using bottom-up approaches is that broader system-wide interactions between processes are not fully represented and some factory-level processes could be missed from scope. Alternatively, Chordia et al. (2021) adopted a top-down approach where they used environmental permit data for a large-scale LIB production facility to scale the factory-level production data to unit process level. Top-down approaches such as those adopted in Chordia et al. (2021) usually represent a broader scope, but potentially lack

precision in estimating the process-specific energy demand. Thus, there are gaps in understanding how cell design influences energy demand in production, and with automakers designing cells for specific applications there are no means or methods to assess the environmental impacts of the wide variety of cell types used in various BEV applications.

In this study, we present a parameterization methodology that links industrial-scale energy demand with cell design parameters, spans a broad range of cell formats and NMC chemistries, and relies on a small set of key parameters to remain simple to apply while retaining flexibility and relevance. The approach combines bottom-up and top-down perspectives for LCA modeling of LIBs by connecting gigafactory-level energy demand with specific cell design characteristics. We demonstrate its applicability across several NMC cell types, showing how variations in design parameters translate into different environmental impacts. The results provide LCA practitioners with cell-specific data for diverse configurations and offer cell design experts insights into the environmental implications of their design choices.

2 | METHODS

This study builds on our prior published work on a cell design computation model (CCM) (Chordia, Wikner et al., 2022) and a life cycle inventory model for large-scale LIB production facility referred to as the "gigafactory" model (Chordia et al., 2021). The core of the methodology is the integration of top-down and bottom-up approaches to develop an LCA model representing cell production at gigafactory scale. The gigafactory model quantifies production-related aspects such as energy consumption, chemical usage, and material losses (recyclable scrap, waste, and emissions), calibrated to a facility with an annual capacity of 16 GWh of NMC-based cells, irrespective of format. These factory-level flows are then linked to cell options generated via the CCM. The CCM provides both composition data (mass distribution of components) and design data (e.g., electrode area and cell energy), yielding a range of plausible configurations for testing the approach. Factory-level energy demand is normalized to unit processes (top-down), while cell mass composition from the CCM is linked to these processes (bottom-up). The central contribution is not new energy demand values, but the methodological link between design parameters and production energy demand under industrial conditions. This parameterization reproduces gigafactory models tailored to each cell type: although annual factory energy use remains constant, the number of cells produced varies by design, leading to cell-type-specific differences in assembly energy and other flows. Finally, we assess the environmental impacts of the modeled cells to demonstrate how design variations influence life cycle outcomes. Specifically, our methodology differs from Clos, Ventura Silva et al. (2025) such that we employ a top-down approach for modeling energy demand and a bottom-up approach for material demand, whereas they do the opposite. Further, we use 4 unique cell design parameters along with cell mass composition in contrast to 20.

In LCA, normalization may refer to dividing the impact assessment results by a reference value to contextualize them, thereby producing a dimensionless result. However, normalization can also describe the process of relating the inflows and outflows of an activity (unit process) to the reference flow. This study applies the latter definition. It assumes that the selected cell design parameters are the primary drivers of energy demand in the relevant production processes. Based on these assumptions, the resulting LCI is modeled in LCA software to conduct the environmental impact assessment. In this section, a generic NMC LIB cell composition is first described, followed by CCM, gigafactory model, the parameterization model, and finally the LCA methodology applied in the study. An overview of the overall methodology applied in this study is shown in Figure 1.

2.1 | Cell composition

An LIB cell is composed of several components, the active parts and parts for safety and function. The active parts consist of electrochemical cells composed of a positive electrode (PE) and a negative electrode (NE) immersed in an electrolyte. To minimize the distance between the electrodes, a separator is used, allowing ion transport but is electrically insulating, to prevent internal short circuit. The electrodes are porous structures coated on a thin metal foil acting as current collectors and providing mechanical stability. The porous structure is composed of the active electrode material, material for improved conductivity and a binder to hold the porous structure together. The thickness of the porous layer, and the type and amount of active material determines the usable capacity per unit area of the electrode.

The PE works as a cathode during discharge and the NE as an anode. During charging, the reactions are reversed, and the PE works as an anode and the NE as a cathode (Newman & Thomas-Aleya, 2004). We use the terms PE and NE when referring to the complete positive or negative electrode assembly, respectively, including the active materials, additives, binders, and metal foils (Renner, 2007). The negative electrode's active material or the NAM is graphite, and the PAM is NMC with varying transition metal composition. A typical LIB cell structure is like that of a sandwich, where layers of electrodes and separators are rolled into a cylindrical or flattened roll, enclosed in a casing and filled with electrolyte. The spiral structure is colloquially referred as a "jelly roll."

2.2 | Cell design computation model and the gigafactory model

The original CCM, presented in Chordia, Wikner et al. (2022), is developed only for cylindrical cells and has been updated to include prismatic cells for this study. At this stage, the CCM itself is a work in progress, being further developed to accommodate additional chemistries and formats
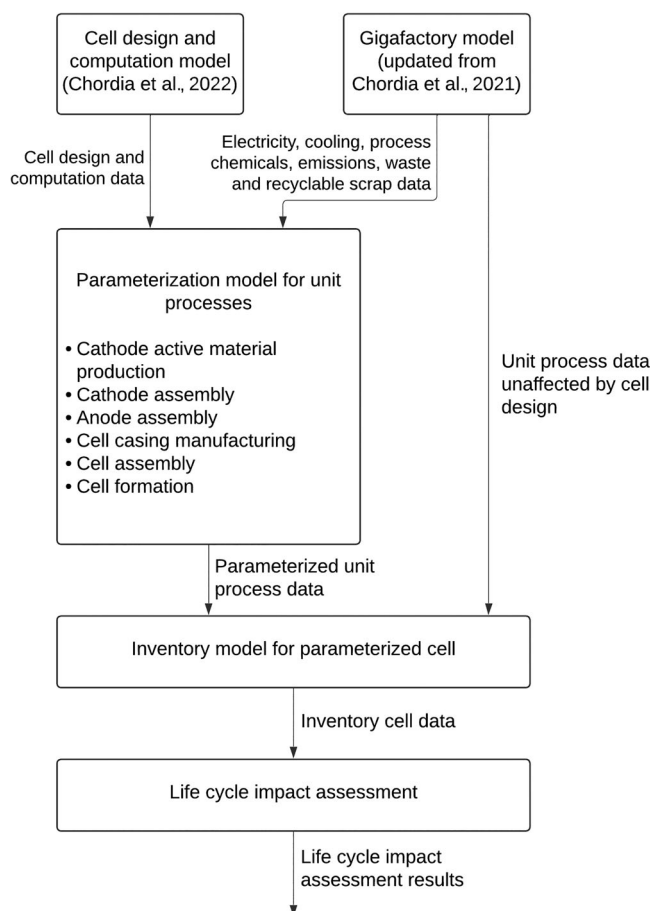
FIGURE 1 Overview of the workflow in the study including the parameterization methodology.

beyond those analyzed here. The CCM calculates the most energy- and power-optimized version of a cell based on a specified capacity for a given cell type. This study focuses on the production of NMC LIB cells for automotive applications, and the CCM is based on generalized design parameters seen in commercial automotive-grade cells. Multiple cell formats (including changes in internal cell design), NMC chemistries, and performance optimizations are modeled to cover a broad range of cell types. Specifically, two cylindrical cell formats (21700 and 18650) and two prismatic cell formats (PHEV2 and BEV2) are modeled. In the PHEV2 cell format, a variation with a modified internal design is modeled—single- and four-jelly rolls. The choice between single- and multiple-jelly rolls reflects trade-offs among energy density, power performance, thermal behavior, and manufacturability. A single-jelly roll maximizes gravimetric and volumetric energy density by reducing inactive material, but longer electrodes in large cells increase resistance, thermal gradients, and risk of mechanical defects. Dividing the electrode into multiple shorter rolls mitigates these issues by reducing transport distances, distributing heat more evenly, and improving winding robustness, though at the cost of added inactive components and lower maximum energy density. Such designs can therefore be advantageous in power-oriented or large-format cells where thermal and manufacturing constraints outweigh marginal energy density losses (Ahmadian-Elmi & Zhao, 2024; Baazouzi et al., 2023; Stock et al., 2023; Yeganehdoust et al., 2025). In terms of chemistries, the BEV2 format is modeled with high-, medium-, and low-nickel content, that is, NMC811, NMC532, and NMC111. Lastly, to represent different performance optimizations, an energy- and power-optimized version of each cell is modeled with the same cell capacity. In our modeling, the distinction between "power" and "energy" cells arises from electrode thickness and porosity rather than the total active-material mass. Power-optimized cells use thinner, more porous electrodes that lower resistance but require more layers, increasing separator and foil demand. Energy-optimized cells use thicker, denser electrodes that achieve the same capacity with fewer layers, reducing separator and foil demand but limiting rate performance. Thus, while active-material mass stays constant, differences in layer structure drive variations in associated component masses, thus reflecting how manufacturers balance energy and power in practice. Table 1 summarizes all the cell types modeled.

The gigafactory model data used in this study is based on the environmental permit data originally reported in Chordia et al. (2021). This dataset includes annual figures for energy demand, processing chemicals, production losses, emissions, and waste generation, corresponding to a facility with a design output of 16 GWh per year. The permit data effectively "locks in" factory-level production flows, which are then normalized to the unit process level for different cell types using the parameterization model. Chordia et al. (2021) employed a top-down modeling approach, partitioning

TABLE 1 List of nickel manganese cobalt oxide lithium-ion battery cells modeled. Each cell listed below is modeled as an energy-optimized and a power-optimized version with the same cell capacity.

Cell geometry	Cell format	NMC	Cell capacity (Ah)	Cell energy (Wh/cell)
Cylindrical	21700	811	4.2	15.4
	18650	811	2.8	10.2
Prismatic	PHEV2, 4 JR	811	38.3	139.8
	PHEV2, 1 JR	811	49.5	180.7
	BEV2	811	124.3	453.7
	BEV2	532	124.3	453.7
	BEV2	111	124.3	453.7

factory-level data based on the annual storage capacity of two cell types produced at the facility. In contrast, this study assumes the production of a single cell type at the factory and rescales the gigafactory data according to cell design parameters unique to each cell type (Table 1). Due to the differences in cell type, each set of unit process inventory represents a unique production model specific for that cell. In practical terms this implies that although the gigafactory "locks-in" the flows at the factory level, the differences in cell type and in turn cell design parameters leads to cell-specific models. This approach avoids the uncertainty associated with selecting partitioning principles for different production processes and instead uses cell design as the primary basis for scaling factory-level data. The gigafactory model assumes electricity as the main energy source for all cell assembly and production processes. Heating requirements are met through electrically powered systems and waste heat recovery, with the energy used for heating included in the total electricity demand. There are also cooling requirements, which are sourced externally and modeled as supplied from adsorption chillers operating on a global average of natural gas-based heat for a high emission scenario and operating on Swedish district heating for a low emission scenario.

2.3 | Parameterization model

The primary objective of the parameterization model is to calculate the energy demand of all intermediate cell assembly and production processes at the unit process level for the cell types listed in Table 1. This is achieved by linking the energy demand of each production and assembly step to a relevant cell design parameter, thereby integrating both bottom-up and top-down modeling approaches within the LCA framework. The methodology unfolds in three key steps:

First, the cell-level data for each cell type in Table 1 is scaled-up to match the gigafactory's annual output of 16 GWh. This involves using scaling equations (Equations 1–11) to convert cell-level data to match the factory output. For this the number of cells produced annually is calculated based on the energy per cell (Wh/cell). Then using this, parameters such as electrode area, solvent mass, electrode slurry mass, and cell casing area are scaled at the factory level, also accounting for production losses. This step represents a bottom-up modeling approach. *Second*, the energy demand of each production and assembly step is linked to specific cell parameters. These linkages are established through a review of technical literature on cell production and informed engineering judgment. This step forms the bridge between the bottom-up data and the top-down gigafactory model. *Third*, the annual energy demand reported in the gigafactory model is normalized to the unit process level by the linked cell parameters. This normalization represents the top-down component of the modeling approach. Steps two and three are summarized in Table 2, which presents the linking cell design parameters, and the normalization equations used to calculate energy demand at the unit process level for each production and assembly step. The annual energy demand values from the gigafactory model are provided in Supporting Information S1. Additionally, all cell mass compositions and design parameters derived from the CCM and the process-specific production losses (*L*) are also reported in the SI.

Step 1: Scaling cell level flows to factory output

To calculate the number of cells produced per year (N_{Cell}), the factory size S (GWh) is divided by the cell energy (E_{Cell}, Wh/cell). In the current study the factory (*S*) is set to 16 GWh/year. The value of E_{Cell} is obtained from the CCM.

$$N_{Cell} = S/E_{Cell} \qquad (1)$$

To calculate the mass of the PAM processed per year (M_{PAM}, kg), the PAM per cell (m_{PAM}, g) is multiplied by N_{Cell}, also including production loss of m_{PAM} (L_{PAM}) at cell level. The value of m_{PAM} is obtained from the CCM.

$$M_{PAM} = \frac{m_{PAM} \times N_{Cell}}{(1 - L_{PAM})} \tag{2}$$

To calculate the PE area processed per year (A_{PE}, m²), the PE area per cell (a_{PE}, m²) is multiplied by N_{Cell}, also including the production loss of a_{PE} (L_{PE}) at cell level. The value of a_{PE} is obtained from the CCM.

$$A_{PE} = \frac{a_{PE} \times N_{Cell}}{(1 - L_{PE})} \tag{3}$$

To calculate the NE area processed per year (A_{NE}, m²), the NE area per cell (a_{NE}, m²) is multiplied by N_{Cell}, also including the production loss of a_{NE} (L_{NE}) at cell level. The value of a_{NE} is obtained from the CCM.

$$A_{NE} = \frac{a_{NE} \times N_{Cell}}{(1 - L_{NE})} \tag{4}$$

To calculate the PE slurry processed per year ($M_{Slurry,PE}$, kg), first the solvent required per PE ($m_{Solvent, PE}$, g) is calculated. The $m_{Solvent,PE}$ is calculated by multiplying the binder mass per PE ($m_{Binder,PE}$, g) by 16, since the solvent to binder ratio is 16:1 (Knehr et al., 2022). The value of $m_{Binder, PE}$ is obtained from the CCM.

$$m_{Solvent,PE} = m_{Binder,PE} \times 16 \tag{5}$$

Then, $M_{Slurry,PE}$ is calculated by multiplying the sum of PAM (m_{PAM}), binder ($m_{Binder,PE}$), and solvent ($m_{Solvent,PE}$) by N_{Cell}, also including the production loss of PE (L_{PE}) at cell level.

$$M_{Slurry,PE} = \frac{(m_{PAM} + m_{Binder,PE} + m_{Solvent,PE}) \times N_{Cell}}{(1 - L_{PE})} \tag{6}$$

To calculate the PE solvent (*N*-methyl-4-pyrrolidone or NMP) used per year ($M_{Solvent}$, kg), solvent per PE ($m_{Solvent,PE}$) is multiplied by N_{Cell}, also including the production loss of PE (L_{PE}) at cell level.

$$M_{Solvent} = \frac{m_{Solvent} \times N_{Cell}}{(1 - L_{Solvent})} \tag{7}$$

To calculate the NE slurry processed per year ($M_{Slurry,NE}$, kg), first the solvent required per NE ($m_{Solvent,NE}$, g) is calculated. The $m_{Solvent,NE}$ is calculated by multiplying the binder mass per NE ($m_{Binder,NE}$, g) by 40, since the solvent to binder ratio is 40:1 (Knehr et al., 2022). The value of $m_{Binder,NE}$ is obtained from the CCM.

$$m_{Solvent,NE} = m_{Binder,NE} \times 40 \tag{8}$$

Then, $M_{Slurry,NE}$ is calculated by multiplying the sum of NAM (m_{NAM}), binder ($m_{Binder,NE}$), and solvent ($m_{Solvent,NE}$) by N_{Cell}, also including the loss of NE (L_{NE}) at cell level.

$$M_{Slurry,NE} = \frac{(m_{NAM} + m_{Binder,NE} + m_{Solvent,NE}) \times N_{Cell}}{(1 - L_{NE})} \tag{9}$$

The cell casing area processed per year (A_{Casing}, m²) is calculated by multiplying the casing area per cell (a_{Casing}, m²) by N_{Cell}, including the loss of cell casing a_{Casing} (L_{Casing}) at cell level. The value of a_{Casing} is obtained from the CCM.

$$A_{Casing} = \frac{a_{Casing} \times N_{Cell}}{(1 - L_{Casing})} \tag{10}$$

To calculate the mass of electrolyte processed per year ($M_{Electrolyte}$, kg), the mass of electrolyte per cell ($m_{Electrolyte}$, g) is multiplied by N_{Cell}, also including the production loss of $m_{Electrolyte}$ ($L_{Electrolyte}$) at cell level. The value of is obtained from the CCM.

$$M_{Electrolyte} = \frac{m_{Electrolyte} \times N_{Cell}}{(1 - L_{Electrolyte})} \tag{11}$$

Steps 2 and 3: Linking cell design and production energy demand and the normalizing equations

Table 2 summarizes Steps 2 and 3 in the parameterization model. Here, the cell parameters and the energy-demanding processes in the cell production are linked, and the normalizing equations to calculate the energy demand at the unit process level ($\bar{E}$) are presented.

TABLE 2 Summary of the linked cell-specific parameter and the normalizing equation for each energy-demanding step in cell production and assembly. The corresponding energy demand values used for the normalizing equation are reported in Supporting Information S1.

Energy-demanding step (x)	Linked cell parameter	Normalizing equation ($\overline{E_x} =$)
Positive active material production unit process		
Calcination	Mass of PAM	$\dfrac{E_{\text{Calcination}}}{M_{\text{PAM}}}$
Other processes	Mass of PAM	$\dfrac{E_{\text{Other processes}}}{M_{\text{PAM}}}$
Positive electrode assembly unit process		
Slurry mixing	Mass of PE slurry	$\dfrac{E_{\text{Slurry mixing, PE}}}{M_{\text{Slurry, PE}}}$
NMP refining	Mass of NMP	$\dfrac{E_{\text{NMP refining,PE}}}{M_{\text{Solvent}}}$
Coating and pressing	Area of the PE foil	$\dfrac{E_{\text{Coating and pressing,PE}}}{A_{\text{PE}}}$
Calendaring	Area of the PE foil	$\dfrac{E_{\text{Calendaring,PE}}}{A_{\text{PE}}}$
Slitting and rewinding (cylindrical)	Area of the PE foil	$\dfrac{E_{\text{Slitting and rewinding,PE}}}{A_{\text{PE}}}$
Notching (prismatic)	Area of the PE foil	$\dfrac{E_{\text{Notching,PE}}}{A_{\text{PE}}}$
Vacuum drying	Area of the PE foil	$\dfrac{E_{\text{Vacuum drying,PE}}}{A_{\text{PE}}}$
Dry room	Area of the PE foil	$\dfrac{E_{\text{Dry room,PE}}}{A_{\text{PE}}}$
Negative electrode assembly unit process		
Slurry mixing	Mass of NE slurry	$\dfrac{E_{\text{Slurry mixing, NE}}}{M_{\text{Slurry, NE}}}$
Coating and pressing	Area of NE foil	$\dfrac{E_{\text{Coating and pressing,NE}}}{A_{\text{NE}}}$
Calendaring	Area of NE foil	$\dfrac{E_{\text{Calendaring,NE}}}{A_{\text{NE}}}$
Slitting and rewinding (cylindrical)	Area of NE foil	$\dfrac{E_{\text{Slitting and rewinding,NE}}}{A_{\text{NE}}}$
Notching (prismatic)	Area of NE foil	$\dfrac{E_{\text{Notching,NE}}}{A_{\text{NE}}}$
Vacuum drying	Area of NE foil	$\dfrac{E_{\text{Vacuum dyring,NE}}}{A_{\text{NE}}}$
Dry room	Area of NE foil	$\dfrac{E_{\text{Dry room,NE}}}{A_{\text{NE}}}$
Cell casing manufacturing unit process		
Stamping	Area of cell casing	$\dfrac{E_{\text{Stamping}}}{A_{\text{Casing}}}$
Cell assembly unit process		
Electrolyte feeding	Mass of electrolyte	$\dfrac{E_{\text{Electrolyte feeding}}}{M_{\text{Electrolyte}}}$
Cell assembly	Cell energy	$\dfrac{E_{\text{Cell assembly}}}{E_{\text{Cell}}}$
Winding	Area of the PE foil	$\dfrac{E_{\text{Winding}}}{A_{\text{PE}}}$
Stacking	Area of the PE foil	$\dfrac{E_{\text{Stacking}}}{A_{\text{PE}}}$
Dry room	Mass of electrolyte	$\dfrac{E_{\text{Dry room, assembly}}}{M_{\text{Electrolyte}}}$
Cell formation unit process		
Formation	Cell energy	$\dfrac{E_{\text{Formation}}}{E_{\text{Cell}} \times (1 - L_{\text{Cell}})}$

TABLE 3 Electricity and cooling demand in cell production reported per cell and per kWh$_{cell}$. The values for both performance-optimized variants are identical hence not reported separately.

Geometry	Format	NMC	Electricity (kWh)		Cooling (MJ)	
			Per cell	Per kWh$_{cell}$	Per cell	Per kWh$_{cell}$
Cylindrical	21700	811	0.9	61-63	1.6	107
	18650	811	0.6	61-63	1.1	107
Prismatic	PHEV2 4JR	811	8.7	61-63	15	107
	PHEV2 1 JR	811	11.2	61-63	19.3	107
	BEV2	811	28.2	61-63	48.6	107
	BEV2	532	28.5	61-63	48.6	107
	BEV2	111	28.5	61-63	48.6	107

2.4 | Inventory model and impact assessment scope

To provide illustrative results from the parameterization, we perform cradle-to-gate LCAs of the different NMC cells. This includes raw material extraction and production, cell precursor production, cell component assembly and manufacturing, and handling of production waste and scrap at site. As the main technical function of an energy storage device such as an LIB cell is to store (and expend) energy, a functional unit of 1 kWh theoretical cell storage capacity (referred hereafter as 1 kWh$_{cell}$) is used to compare the cell types modeled in the study, as is common and relevant in LCAs of batteries (Peters, 2023). The study adopts an attributional type of inventory modeling, in which environmentally relevant inputs and outputs are "attributed" to the product life cycle (Finnveden et al., 2009). Global averages for material and energy inputs to the gigafactory are considered to provide a global estimate of the environmental impacts linked to LIB cell production. In addition, a low-carbon intensive scenario (represented by the Swedish energy mix) is modeled for the energy supply mix to contrast and compare to the global average. The background system is modeled using the Ecoinvent database version 3.9.1 (Steubing et al., 2016; Wernet et al., 2016).

Impact assessment is performed to assess climate change and resource use impacts. The former is often reported in LCAs of LIBs and also amongst the recommended impact categories for LCAs of batteries (European Union, 2023). The climate change impacts are assessed using IPCC 2021 characterization factors (IPCC, 2023). The resource use impacts are assessed taking a long-term resource scarcity perspective. For this, the crustal scarcity indicator (CSI) is used, which is based on the concentration of metals, minerals, ores, and other materials in the earth's crust (Arvidsson et al., 2020).

3 | RESULTS AND ANALYSIS

3.1 | Energy demand in cell production

Table 3 presents the results for electricity and cooling demand per cell (item) and per kWh$_{cell}$ for all the cell types modeled in this study. These results are compared to the studies discussed in the introduction. Knehr et al. (2024), Jinasena et al. (2021), and Degen and Schütte (2022) report energy consumption starting from the mixing step in electrode production, whereas the current study includes the PAM production as well. This processing step alone accounts for about 18% of the production energy in the factory model represented in this study. Additionally, our model also includes processes such as cell casing manufacturing, electrolyte mixing, water treatment, and several other factory-level processes such as utilities, building and infrastructure support functions, warehouses, and material handling in the calculation of the overall energy demand; thus, representing a broader scope. Also indicating the potential benefits of taking a top-down approach to modeling. For the same scope as mentioned in Knehr et al. (2024), Jinasena et al. (2021), and Degen and Schütte (2022), the current study estimates approximately 43 kWh/kWh$_{cell}$ of electricity and 70 MJ/kWh$_{cell}$ of cooling energy demand. Knehr et al. (2024) and Degen and Schütte (2022) state that heat requirement in cell production is sourced from natural gas. Whereas the facility represented in this study recovers heat from the operating machinery and additional heat is supplied from electrically powered heating. The cooling demand is also met with electricity, through adsorption chillers, but reported separately for transparency and modeling flexibility. These aspects, apart from the broader scope of cell production considered in this study, explain the higher electricity demand reported in this study. Specifically, Degen and Schütte (2022), calculate energy demand based on the machine(s) with a lowest throughput in terms of producible cell capacity, whereas Knehr et al. (2024) calculate energy demand based on 60%–80% of the maximum machine rated power depending on the type of production process. In this study, the energy demand is calculated by incorporating the load factor, which adjusts the maximum

machine power rating to reflect actual usage over time, and the diversity factor, which accounts for the likelihood that multiple machines will not operate at their peak simultaneously.

In terms of energy demand per cell, this study reports values in the range of 1–30 kWh/cell for electricity demand, and 2–50 MJ/cell for cooling energy. This high variability is linked to the size of the cell and its internal design. The energy demand in production of energy- and power-optimized versions of the same cell type is similar. When normalized per kWh of storage capacity (kWh_{cell}), the energy demand associated with LIB production shows limited variation across different NMC cell types. This is because higher-capacity cells, achieved through thicker electrodes or larger formats, contain more electrode material and store proportionally more energy, while the energy required to process each unit of electrode material remains similar. Consequently, as the total production energy increases with the amount of electrode material, it increases in line with the increase in stored energy, resulting in a relatively stable energy demand per kWh_{cell} across cell types. In contrast, when energy demand is assessed per cell, substantial variation emerges due to design-specific factors such as form factor, electrode thickness, and assembly configuration. Factors such as form factor, electrode thickness, and assembly configuration directly influence the energy requirements for material processing, coating, drying, and formation. These processes are sensitive to the physical design of the cell but do not scale with the energy content of the cell, resulting in higher variability in energy demand when expressed per cell. The exclusive focus on NMC chemistries in this study further reduces variability in energy demand per kWh_{cell} across cell types. NMC-based cells share similar positive electrode compositions, electrode formulations, and gravimetric and volumetric energy densities. These shared characteristics constrain the variation in active material mass required to achieve a given capacity. Moreover, the electrochemical properties of NMC chemistries, such as voltage, specific capacity, and processing conditions, are relatively consistent, thereby minimizing differences in production energy demand when assessed per kWh_{cell}. As a result, the observed variation in energy demand per kWh is significantly lower than would be expected in cross-chemistry comparisons (e.g., NMC vs. LFP), where differences in material properties and processing requirements are more pronounced.

3.2 | Climate and resource impacts

The climate impacts from material use varies between 50 and 84 kg CO_2-eq./ kWh_{cell}, whereas the production (electricity and cooling) impacts are ~53 kg CO_2-eq./kWh_{cell}. For low-carbon intensive energy mix, the production impacts reduce to ~5 kg CO_2-eq./kWh_{cell}. These results show that differences in cell design such as format, chemistry, and number of jelly rolls can notably affect the impacts from material use. However, energy use-related impacts from cell NMC LIB cell production tend to vary little when measured per kWh. Thus, the choice of materials and its supply source is an important aspect when quantifying the impacts from LIB production, as also highlighted in other studies (Istrate et al., 2024; Kallitsis et al., 2024). The variation in impacts from material inputs points to the efficiency in design of some cell types over others.

Overall, resource use impacts vary between 5.5E4 and 9.5E4 kg Si-eq./kWh_{cell}. Within that, PAMs such as nickel sulfate, cobalt sulfate, lithium hydroxide, lithium carbonate, and copper foil dominate the resource use impacts. For medium and low-nickel-content chemistries, impacts from cobalt sulfate dominate. Power -optimized versions across all formats have higher impacts as compared to the energy-optimized cells, linked mainly to copper use.

3.3 | Cell format

Figure 2 shows the climate impacts for the four cell formats modeled in the study for both performance optimizations. Results are shown only for NMC811 PAM and low-carbon energy input scenario. Cylindrical cells modeled in this study have lower climate impacts compared to prismatic cells. While the impacts linked to energy demand are similar overall, the key differentiator lies in choice of materials, in particular that of the cell casing. This is driven by two specific modeling assumptions: (1) the choice of casing material and (2) the use of global averages to model material inputs. Cylindrical cell casings are modeled as nickel-plated stainless steel, though some manufacturers use aluminum for the casing body. In contrast, all prismatic cells are modeled with an aluminum casing, which aligns with common industry practices aimed at reducing cell weight.

To model the upstream processes for steel and aluminum production, market processes available in Ecoinvent database are used. The market processes in Ecoinvent represent a mix of similar outputs from different transforming processes located within the geographical limitation of the product's market (Wernet et al., 2016). Based on this, the market for steel and aluminum production is modeled containing approximately 75% and 70% inputs from primary raw material extraction and production, respectively, with the balance of inputs coming from secondary sources. In Ecoinvent, primary aluminum production has higher climate impact per unit mass compared to primary steel production when their global averages are compared. Primarily, aluminum production is an electricity-demanding process due to the smelting step, where a large amount of electricity is continually needed to electrolytically reduce the aluminum oxide to form aluminum (Brough & Jouhara, 2020). If the casing for cylindrical cells is also made of aluminum, the overall impacts from cylindrical cell production would be higher than what is calculated here, linked to higher impacts from primary aluminum production. However, if aluminum is produced using renewable energy as a source, the climate impact from aluminum production and hence cell casing could be much lower. Additionally, production impacts of secondary aluminum are considerably lower than primary
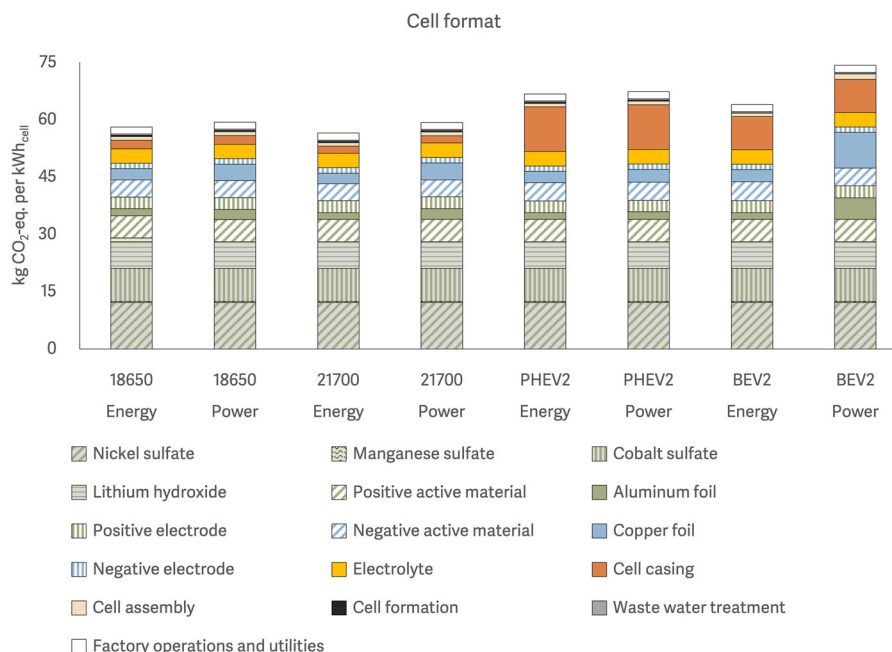
FIGURE 2 Climate impacts per kWh of cell production. The figure shows results for NMC811 positive active material chemistry cells produced using low-carbon intensity energy mix. The figure highlights the differences in production impacts of various cell formats and the effect of energy and power optimization for each cell type. The color scheme is kept consistent across all figures.

aluminum (Das & Yin, 2007; Schlesinger, 2006). Thus, using secondary aluminum in cell components where possible, without compromising the cell performance, is another way to reduce impacts from cell production.

Further, the volumetric efficiency of cylindrical cells is generally better than that of prismatic cells (Sit et al., 2004). Hence, more casing mass is used in the case of prismatic cells for packing the same mass of active materials. Thus, if the casing material for the cylindrical cells is changed to aluminum, the impacts compared to prismatic cells would still be lower due to the lower cell casing mass used per kWh in cylindrical cells. However, it should be noted that at the battery pack level, the prismatic cells might offer better packing and thermal conductivity than cylindrical cells (Löbberding et al., 2020).

3.4 | Energy- and power-optimized cells

Figure 2 also shows the climate impacts for the energy- and power-optimized versions of the cells modeled. The results show that the power-optimized cells have higher impacts compared to the energy-optimized cells for all cell format and chemistry variants considered even though the energy demand in production is similar to that of energy-optimized cells. As power-optimized cells are designed to achieve higher power density (instead of energy density), they have thinner electrodes but a larger electrode surface area to reach the same capacity as that of comparable energy-optimized cells. The foil surface area of both current collectors, made of aluminum for the PE and copper for the NE, is larger than that of comparable energy-optimized cells. As a result of this, power-optimized cells have higher current collector mass compared to energy-optimized cells, which results in higher environmental impacts.

3.5 | Internal cell design

Figure 3 shows the climate and resource impacts of power-optimized PHEV2 cells of varying internal design, that is, single- versus four-jelly rolls. The climate impacts are shown on the primary axis. The single-jelly roll cell has an energy capacity of 180 Wh per cell and the four-jelly roll cell has an energy capacity of 140 Wh per cell. Both cells weigh approximately 850 g. However, despite similar mass of the cell including the active materials, the single-jelly roll has lower climate impacts, linked to climate impacts of electrode foils and casing material production. This highlights the superior volumetric efficiency of the single-jelly roll cell, which makes it preferable from a climate impact perspective.
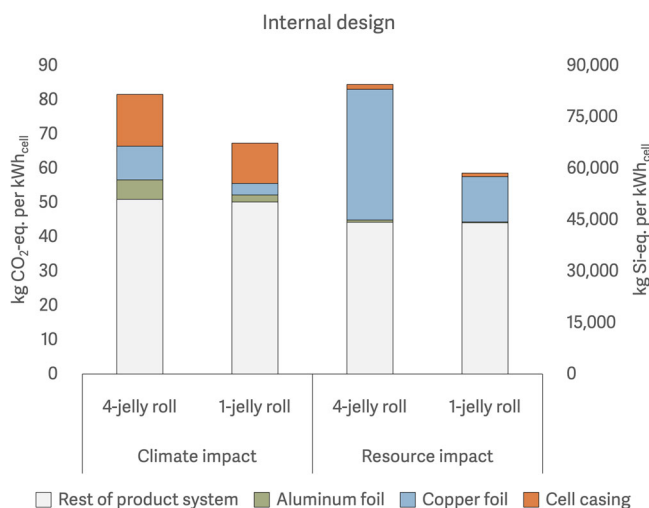
FIGURE 3 Climate and resource use impacts per kWh of cell production. The figure shows results for PHEV2 cell of NMC811 positive active material chemistry produced using low-carbon intensity energy mix. The figure highlights the differences in production impacts due to changes in internal cell design.
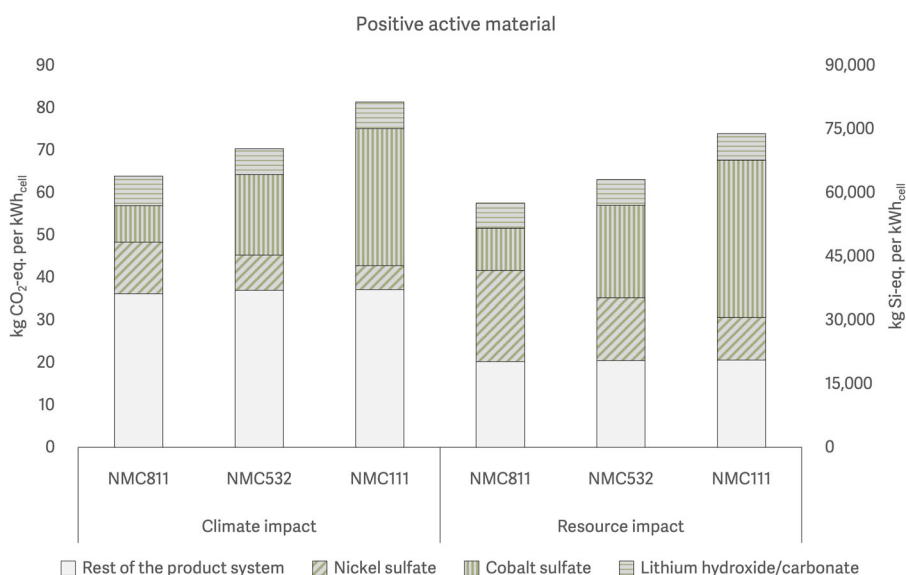

FIGURE 4 Climate and resource use impacts per kWh of cell production. The figure shows results for BEV2 cell produced using low-carbon intensity energy mix. The figure highlights the differences in production impacts due to changes in positive active material chemistry.

Resource impacts, shown on the secondary axis highlight the impacts from the copper foil and the nickel sulfate. The main differentiator between the two internal cell designs is the higher amount of copper foil used in the four-jelly roll design. Once again pointing to the impacts of internal cell design on the cell.

3.6 | Positive active material chemistry

Variations in climate impacts due to changes in cell chemistry can be seen in Figure 4. Specifically, the results for a BEV2 format cell with varying NMC composition are highlighted. The NMC811 chemistry with the highest-nickel content (i.e., the lowest share of cobalt) has lower impacts compared to the lower-nickel-content chemistries (NMC532 and NMC111). The reason for this is higher impacts of cobalt compared to nickel and manganese per unit mass.

In terms of long-term resource scarcity (Figure 4), a similar trend as for climate impacts is observed related to impacts from cobalt extraction. In addition, the power-optimized cells show notably higher impacts compared to the energy-optimized cells of the same format and chemistry due to the higher share of copper use in power-optimized cells.

3.7 | Limitations

There are several limitations in the current study. The energy demand calculations for the parameterization model are representative of production in a 16 GWh/year facility. The model currently does not parameterize based on changes in production volume. However, as seen in the study by Knehr et al. (2024)—whose calculations for energy demand covered facilities ranging between 5 and 50 GWh/year—the effect of scale might not be considerable beyond a point in highly optimized large-scale LIB production facilities. Still, this aspect needs to be explored further.

The second limitation is that the CCM model used to calculate the data for the cells covered in this study is based on teardown reports for automotive-grade cells and might not be relevant for other applications, such as consumer electronics. Ideally, company data for cells would be best suited for validating the CCM. Further, the inventory model for the parameterized cells needs to be further validated with corresponding cell production data. However, such data is usually proprietary and hard to access. We encourage LCA practitioners modeling cell production processes to compare using the presented parameterization methodology and highlight the differences.

The third limitation concerns the simplifications made when linking cell parameters to energy-demanding steps. Cell production is complex and sensitive to changes in format and size. This study simplifies several steps for brevity, such as sealing, welding, and handling during cell assembly process, which can differ between cylindrical and prismatic cells and add variation in per cell energy demand. However, as seen in other production stages, these differences tend to even out when assessed per kWh_{cell}.

In this study, the functional unit is 1 kWh storage capacity. However, normalizing over the power capability (kW) instead of the energy capability (kWh) might change the results. For many applications, the power-to-energy ratio is an important measure to evaluate whether a cell is applicable for the intended use. However, the most common functional unit used in LCA studies on LIBs is kWh_{cell} and to ensure comparability kWh_{cell} has thus been used in this work as well. Lastly, this study only reports and discusses climate and resource impacts. Assessing other environmental impacts could present more insights on cell design and its relation to environmental impacts and possible mitigation measures.

4 | CONCLUSION

This study contributes to literature on LCA of LIBs by assessing the impact of cell type on energy demand and the associated climate and resource impacts. This is accomplished by means of a parameterization methodology that links cell production processes to relevant cell design parameters. Further, by implementing the methodology for several LIB cell types, we also supplement LCA literature with unit process data for 14 cell types which have not been covered in the LCA literature in detail before. The novelty of the study lies in developing a parameterized framework that explicitly connects gigafactory scale energy demand with cell design parameters. Unlike earlier studies that focus on a single format or chemistry, our approach covers a broad range of cell types and NMC chemistries within a consistent methodology, while relying on a small set of carefully selected parameters.

In terms of energy demand in cell production, there is high variability when the results are reported per cell, linked primarily to the overall size of the cell and its internal components. However, the variability in energy demand is low when energy demand is reported per kWh_{cell} due to similar energy density of the cells assessed. Power-optimized cells tend to have higher climate and resource impacts compared to energy-optimized cells of the same capacity, format, and chemistry when using kWh_{cell} as the functional unit. From a long-term resource scarcity perspective, impacts due to higher copper use in power-optimized cells are noteworthy for the automotive industry due to the importance of copper in the industrialized world. Copper is used in many applications and can be expected to rise in demand for BEVs, so reducing copper use could be an avenue for reducing resource scarcity from cell production.

Climate impacts linked to material inputs vary notably across all cell types assessed, while the range of impacts from energy use is low when calculated per kWh. This points to the importance of material selection and its supply source. An example of this is seen in the case of cylindrical cell casing bodies that could be manufactured using aluminum or steel. Due to higher impacts from producing aluminum compared to steel, for current global averages, the cell casings with aluminum body have higher impacts compared to similar cells with steel bodies. However, this can be offset using low-carbon intensive sources for primary aluminum production or using secondary aluminum as input. Lastly, better volumetric efficiency in a cell yields lower climate impacts per kWh_{cell} as seen in the case of jelly roll packing in prismatic cells. Hence, internal design of a cell must be considered when assessing impacts from cell production.

ORCID

Mudit Chordia https://orcid.org/0000-0002-9228-8579
Anders Nordelöf https://orcid.org/0000-0002-7455-7341
Rickard Arvidsson https://orcid.org/0000-0002-9258-0641

REFERENCES

Ahmadian-Elmi, M., & Zhao, P. (2024). Review of thermal management strategies for cylindrical lithium-ion battery packs. *Batteries, 10*(2), 50.

Arvidsson, R., Söderman, M. L., Sandén, B. A., Nordelöf, A., André, H., & Tillman, A.-M. (2020). A crustal scarcity indicator for long-term global elemental resource assessment in LCA. *The International Journal of Life Cycle Assessment, 25*(9), 1805–1817. https://doi.org/10.1007/s11367-020-01781-1

Baars, J., Cerdas, F., & Heidrich, O. (2023). An integrated model to conduct multi-criteria technology assessments: The case of electric vehicle batteries. *Environmental Science & Technology, 57*(12), 5056–5067.

Baazouzi, S., Feistel, N., Wanner, J., Landwehr, I., Fill, A., & Birke, K. P. (2023). Design, properties, and manufacturing of cylindrical Li-ion battery cells—A generic overview. *Batteries, 9*(6), 309.

Birke, K. P., & Demolli, S. (2018). Lithium-ion cells: Discussion of different cell housings. In *Modern battery engineering* (pp. 31–41). World Scientific. https://doi.org/10.1142/9789813272163_0002

Bouter, A., & Guichet, X. (2022). The greenhouse gas emissions of automotive lithium-ion batteries: A statistical review of life cycle assessment studies. *Journal of Cleaner Production, 344*, 130994. https://doi.org/10.1016/j.jclepro.2022.130994

Brough, D., & Jouhara, H. (2020). The aluminium industry: A review on state-of-the-art technologies, environmental impacts and possibilities for waste heat recovery. *International Journal of Thermofluids, 1–2*, 100007. https://doi.org/10.1016/j.ijft.2019.100007

Chabot, V., Farhad, S., Chen, Z., Fung, A. S., Yu, A., & Hamdullahpur, F. (2013). Effect of electrode physical and chemical properties on lithium-ion battery performance. *International Journal of Energy Research, 37*(14), 1723–1736. https://doi.org/10.1002/er.3114

Chordia, M., Nordelöf, A., & Ellingsen, L. A.-W. (2021). Environmental life cycle implications of upscaling lithium-ion battery production. *The International Journal of Life Cycle Assessment, 26*(10), 2024–2039. https://doi.org/10.1007/s11367-021-01976-0

Chordia, M., Wickerts, S., Nordelöf, A., & Arvidsson, R. (2022). Life cycle environmental impacts of current and future battery-grade lithium supply from brine and spodumene. *Resources, Conservation and Recycling, 187*, 106634. https://doi.org/10.1016/j.resconrec.2022.106634

Chordia, M., Wikner, E., & Nordelöf, A. (2022). A model platform for solving lithium-ion battery cell data gaps in life cycle assessment. EVS 35 Symposium, Oslo. https://www.diva-portal.org/smash/get/diva2:1920443/FULLTEXT01.pdf

Clos, D. P., Baars, J., Holsten, J., Orangi, S., Cerdas, F., Dilger, N., Zellmer, S., Herrmann, C., & Strømman, A. (2025). A battery modeling platform for broad, consistent, and automated life cycle assessments and cost studies (B-LEAP). *Journal of Industrial Ecology, 29*(4), 1208–1222. https://doi.org/10.1111/jiec.70021

Clos, D. P., Ventura Silva, G., Cerdas, F., Burheim, O., Herrmann, C., & Stromman, A. (2025). Development and validation of scalable energy models for battery cell production processes. *Energy Technology, 13*(8), 2402114. https://doi.org/10.1002/ente.202402114

Das, S. K., & Yin, W. (2007). The worldwide aluminum economy: The current state of the industry. *Journal of the Minerals Metals and Materials Society, 59*, 57–63.

Degen, F., & Schütte, M. (2022). Life cycle assessment of the energy consumption and GHG emissions of state-of-the-art automotive battery cell production. *Journal of Cleaner Production, 330*, 129798. https://doi.org/10.1016/j.jclepro.2021.129798

Degen, F., Winter, M., Bendig, D., & Tübke, J. (2023). Energy consumption of current and future production of lithium-ion and post lithium-ion battery cells. *Nature Energy, 8*(11), 1284–1295. https://doi.org/10.1038/s41560-023-01355-z

Ding, Y., Cano, Z. P., Yu, A., Lu, J., & Chen, Z. (2019). Automotive Li-ion batteries: Current status and future perspectives. *Electrochemical Energy Reviews, 2*(1), 1–28. https://doi.org/10.1007/s41918-018-0022-z

Finnveden, G., Hauschild, M. Z., Ekvall, T., Guinée, J., Heijungs, R., Hellweg, S., Koehler, A., Pennington, D., & Suh, S. (2009). Recent developments in life cycle assessment. *Journal of Environmental Management, 91*(1), 1–21. https://doi.org/10.1016/j.jenvman.2009.06.018

Greenwood, M., Wentker, M., & Leker, J. (2021). A bottom-up performance and cost assessment of lithium-ion battery pouch cells utilizing nickel-rich cathode active materials and silicon-graphite composite anodes. *Journal of Power Sources Advances, 9*, 100055. https://doi.org/10.1016/j.powera.2021.100055

IEA. (2024). Batteries and secure energy transition. https://www.iea.org/reports/batteries-and-secure-energy-transitions

IPCC. (2023). *Climate change 2021 – The physical science basis: Working Group I contribution to the Sixth Assessment Report of the Intergovernmental Panel on Climate Change.* Cambridge University Press. https://doi.org/10.1017/9781009157896

Istrate, R., Mas-Fons, A., Beylot, A., Northey, S., Vaidya, K., Sonnemann, G., Kleijn, R., & Steubing, B. (2024). Decarbonizing lithium-ion battery primary raw materials supply chain. *Joule, 8*, 2992–3016. https://doi.org/10.1016/j.joule.2024.10.003

Jinasena, A., Burheim, O. S., & Strømman, A. H. (2021). A flexible model for benchmarking the energy usage of automotive lithium-ion battery cell manufacturing. *Batteries*, 7(1), 14. https://doi.org/10.3390/batteries7010014

Kallitsis, E., Lindsay, J. J., Chordia, M., Wu, B., Offer, G. J., & Edge, J. S. (2024). Think global act local: The dependency of global lithium-ion battery emissions on production location and material sources. *Journal of Cleaner Production*, 449, 141725. https://doi.org/10.1016/j.jclepro.2024.141725

Knehr, K. W., Kubal, J. J., Nelson, P. A., & Ahmed, S. (2022). Battery performance and cost modeling for electric-drive vehicles (A manual for BatPaC v5.0). https://www.osti.gov/biblio/1877590

Knehr, K. W., Kubal, J. J., Yoon, S., Jeon, H., Roh, W. J., & Ahmed, S. (2024). Energy consumption of lithium-ion pouch cell manufacturing plants. *Journal of Cleaner Production*, 468, 143050. https://doi.org/10.1016/j.jclepro.2024.143050

Löbberding, H., Wessel, S., Offermanns, C., Kehrer, M., Rother, J., Heimes, H., & Kampker, A. (2020). From cell to battery system in BEVs: Analysis of system packing efficiency and cell types. *World Electric Vehicle Journal*, 11(4), 77.

Manthiram, A. (2017). An outlook on lithium ion battery technology. *ACS Central Science*, 3(10), 1063–1069. https://doi.org/10.1021/acscentsci.7b00288

Mekonnen, Y., Sundararajan, A., & Sarwat, A. I. (2016). A review of cathode and anode materials for lithium-ion batteries. SoutheastCon 2016.

Newman, J., & Thomas-Aleya, K. (2004). *Electrochemical systems*. Wiley-Blackwell.

Noh, H.-J., Youn, S., Yoon, C. S., & Sun, Y.-K. (2013). Comparison of the structural and electrochemical properties of layered Li[Ni$_x$Co$_y$Mn$_z$]O$_2$ (x = 1/3, 0.5, 0.6, 0.7, 0.8 and 0.85) cathode material for lithium-ion batteries. *Journal of Power Sources*, 233, 121–130. https://doi.org/10.1016/j.jpowsour.2013.01.063

Perner, A., & Vetter, J. (2015). 8 - Lithium-ion batteries for hybrid electric vehicles and battery electric vehicles. In B. Scrosati, J. Garche, & W. Tillmetz (Eds.), *Advances in battery technologies for electric vehicles* (pp. 173–190). Woodhead Publishing. https://doi.org/10.1016/B978-1-78242-377-5.00008-X

Peters, J. F. (2023). Best practices for life cycle assessment of batteries. *Nature Sustainability*, 6(6), 614–616. https://doi.org/10.1038/s41893-023-01067-y

Regulation (EU). 2023/1542 on batteries and waste batteries, 1–114 (2023). https://eur-lex.europa.eu/legal-content/EN/TXT/PDF/?uri=CELEX%3A32023R1542

Renner, T. (2007). *Quantities, units and symbols in physical chemistry*. The Royal Society of Chemistry. https://doi.org/10.1039/9781847557889

Sankar, T. K., Abhilash, & Meshram, P. (2023). Environmental impact assessment in the entire life cycle of lithium-ion batteries. *Reviews of Environmental Contamination and Toxicology*, 262(1), 5. https://doi.org/10.1007/s44169-023-00054-w

Schlesinger, M. E. (2006). *Aluminum recycling*. CRC Press.

Shin, J., & Lee, Y. K. (2024). Multi-scale mechanical-electrochemical coupled modeling of stress generation and its impact on different battery cell geometries. *Journal of Power Sources*, 595, 234064. https://doi.org/10.1016/j.jpowsour.2024.234064

Sit, K., Li, P. K. C., Ip, C. W., Li, C. W., Wan, L., Lam, Y. F., Lai, P. Y., Fan, J., & Magnuson, D. (2004). Studies of the energy and power of current commercial prismatic and cylindrical Li-ion cells. *Journal of Power Sources*, 125(1), 124–134. https://doi.org/10.1016/S0378-7753(03)00833-4

Steubing, B., Wernet, G., Reinhard, J., Bauer, C., & Moreno-Ruiz, E. (2016). The ecoinvent database version 3 (part II): Analyzing LCA results and comparison to version 2. *The International Journal of Life Cycle Assessment*, 21(9), 1269–1281. https://doi.org/10.1007/s11367-016-1109-6

Stock, S., Hagemeister, J., Grabmann, S., Kriegler, J., Keilhofer, J., Ank, M., Dickmanns, J. L. S., Schreiber, M., Konwitschny, F., Wassiliadis, N., Lienkamp, M., & Daub, R. (2023). Cell teardown and characterization of an automotive prismatic LFP battery. *Electrochimica Acta*, 471, 143341. https://doi.org/10.1016/j.electacta.2023.143341

Wernet, G., Bauer, C., Steubing, B., Reinhard, J., Moreno-Ruiz, E., & Weidema, B. (2016). The ecoinvent database version 3 (part I): Overview and methodology. *The International Journal of Life Cycle Assessment*, 21(9), 1218–1230. https://doi.org/10.1007/s11367-016-1087-8

Yeganehdoust, F., Madikere Raghunatha Reddy, A. K., & Zaghib, K. (2025). Cell architecture design for fast-charging lithium-ion batteries in electric vehicles. *Batteries*, 11(1), 20.

SUPPORTING INFORMATION

Additional supporting information can be found online in the Supporting Information section at the end of this article.